An Energy-based Predictive Control with a Fast Real-Time Current-Tuning for Mono-Inverter Dual-Parallel PMSM Motors in Power Train Application

M. Fadaie[1], K. Abbaszadeh [2]*, and A. Siadatan [3,4]

[1] Department of Electrical Engineering, Faculty of Electrical Engineering, Science and Research Branch, Islamic Azad University, Tehran, Iran (e-mail: mehdi.fadaie.a@gmail.com).

[2] Department of Electrical Engineering, Faculty of Electrical Engineering K. N. Toosi University of Technology, Tehran, Iran (e-mail: abbaszadeh@kntu.ac.ir).

[3] Department of Electrical Engineering, College of Technical and Engineering West Tehran Branch, Islamic Azad University, Tehran, Iran (e-mail: a_siadatan@sbu.ac.ir).

[4] Energy Systems Group, Faculty of Applied Science and Engineering, University of Toronto, Toronto, Ontario, Canada (e-mail: a_siadatan@sbu.ac.ir).

* Corresponding Author

Abstract— **Economic approach and optimization in rail transportation systems led to the introduction of the mono inverter dual parallel motor (MIDP) system. Most researchers introduce the model predictive control (MPC) method to drive this system in order to overcome the problem of load torque inequality on the wheels. But the obtained control signals do not result in the proper operation of the MIDP system, because the cost function is solved online or evaluated by the limited number of control signals. The present paper introduces an energy-based predictive speed control instead of the conventional proportional-integral controller in the outer loop and uses Pontryagin's maximum principle to regulate electrical currents in the inner loop. Since this method solved the quadratic-linear cost functions offline, the control signals of the MIDP system are obtained as linear-parametric functions. After modeling and simplifying the mathematical equations, the introduced method is simulated and compared with conventional Finite and Infinite Control Set-MPC methods. The results indicate the agility and high accuracy of the controllers in both transient and steady states.**

Keywords: **Mono Inverter Dual Parallel (MIDP), Model Predictive Control (MPC), Permanent Magnet Synchronous Motor (PMSM)**

I. INTRODUCTION

THE electric trains in the transportation systems have always been of interest. The high inertia and the slow speed changes as well as the reduction of cost and the volume of electromotive force have become incentives to feed and control two or more motors by a single inverter. Subsequently, the Mono Inverter Dual Parallel (MIDP) systems were introduced to be applied in high inertia devices. The year 1977, namely [1], can be marked as the beginning of research in this field. Based on studies done so far, motor drives in the MIDP systems can be categorized into two groups, including weighting-based control and model-based control. There are two approaches in the weighting-based control. The first is the averaged vector control of motors, which includes the current and voltage space vector averaging technique [2, 3], the averaging of equivalent circuit parameters in the steady state (used only in induction motors) [4], the mean and differential torque control [5-7], and the weighted averaging of control parameters [8]. There are problems with this approach such as the existence of severe and long fluctuations in the current waveforms, dependence of the calculated commands on the motor type and weak stability of the slave motor. Master-Slave (MS) is the second approach, in which the motor is controlled

through the maximum mechanical load at each moment. Since control signals are only generated by the Master motor, eliminating fluctuations and maintaining stable performance of motors are the main concerns [9, 10]. Although the proportional gain set of the system is not simple, the Active Damping Control is used to fix the mentioned problems [11-13]. Despite the simplicity of weighting-based control method, the loop in the slave motor is open, and the optimal operating point depends on the steady state model [14]. The method of reduced linearized feedback has been used on independent torque control in the MIDP system [15]. Although the designed controller could hardly control the system at a single point, it could control the MIDP system under severe unequal load torques.

With the advent of powerful microcontrollers, the Model Predictive Control (MPC) method was used in electrical motor drives. Typically, this method was developed in two ways: Predictive Current Control (PCC) and Predictive Torque Control (PTC), which are applied to Permanent Magnet Synchronous Motor (PMSM) control [16-18], induction motor control [19, 20], and MIDP system control [21, 22]. There are two general approaches in control of MIDP system. The first approach, called the Finite Control Set-Model Predictive Control (FCS-MPC), was applied on two PMSMs and two induction motors in [23, 24] and [25, 26], respectively. This method uses just six well-known voltage vectors in SVPWM (Space Vector Pulse Wide Modulation) to minimize the cost function. These vectors have the same amplitude with an angle difference of 60 degrees relative to each other. Certainly, the lowest value of the cost function is not obtained by six voltage vectors, and it is necessary to consider all of the voltage space vectors. Hence, the Seek and Split-PTC method used a large number of voltage space vectors [27]. In FCS-MPC method, generally, the obtained voltage vectors do not lead to the absolute minimum value of the cost function, and the system constraints do not affect determining the control signal.

The second approach, with a better performance than FCS-MPC, is the Continues Control Set-Model Predictive Control (CCS-MPC) method [28]. Using one of the optimal control methods, it solves the cost function through considering some limitations and system initial conditions. Therefore, it generates the control signals according to the model parameters, the initial condition of the control variables and the state feedback values. Perhaps the pioneer of CCS-MPC is the Optimal Torque Predictive Control method [29, 30]. Among problems of this research, severe fluctuations in the transient state and tendency of the cost function to a non-zero value can be mentioned. In [31], system constraints were used to

determine control signals. However, the control loop of optimal angle displacement not only prolonged the fluctuations of the control variables, but also increased the sensitivity of the method to the motor parameters. Therefore, further studies are needed to introduce a method to obtain optimal control signals for MIDP systems.

This paper presents an analytical comprehensive algorithm for designing current controller of all electrical motors in any structure. Also, an effective speed controller is introduced based on the nominal power and kinetic energy of the motors. The produced control signals in both controllers are linear-parametric functions of the state variables. Thus, the proposed drive technique saves computation time and processing memory, significantly. It considers the transient and steady state of the system and involves the system constraints in the process of generating control signals. The designed speed and current controllers, which are based on the Lagrange method and the Pontryagin's Maximum Principle respectively, are used to develop a cascade structure. Also, the necessary and sufficient condition are considered for controllability of the system at any given time.

This article is organized as follows: In the first part, the model of two PMSM motors will be obtained in a rotor reference frame. In order to measure the validity of the design method of the introduced controllers and their capability in transient conditions, two low-inertial permanent magnet synchronous motors are considered. In the second part, the producing control signals are presented and the necessary and sufficient condition for generating the control signals is examined. Then, in the MIDP system, the simulation results of the proposed method along with their analysis are presented and compared with the two methods of FCS-MPC and Infinite Control Set-Model Predictive Control (ICS-MPC). Finally, conclusion is presented.

II. MIDP SYSTEM DRIVE STRUCTURE

Fig. 1 shows the cascade structure of the MIDP system drive with PMSM motors. Instead of using the conventional proportional-integral controller in the outer loop, $\hat{I}_{qs}$ control signals are generated by the MPC method using the reference speed, the speed measured values and estimated torque of both motors. In the inner loop, the MPC method is employed to generate $\hat{V}_{dq}$ (voltage control signals) by measuring I_{dqs} currents and motor speeds, and the space vector modulation method is used to produce inverter switching commands. In this configuration, the I_{ds} current commands in each motor is considered equal to zero, which maximizes the torque per ampere ratio under equal load torques.
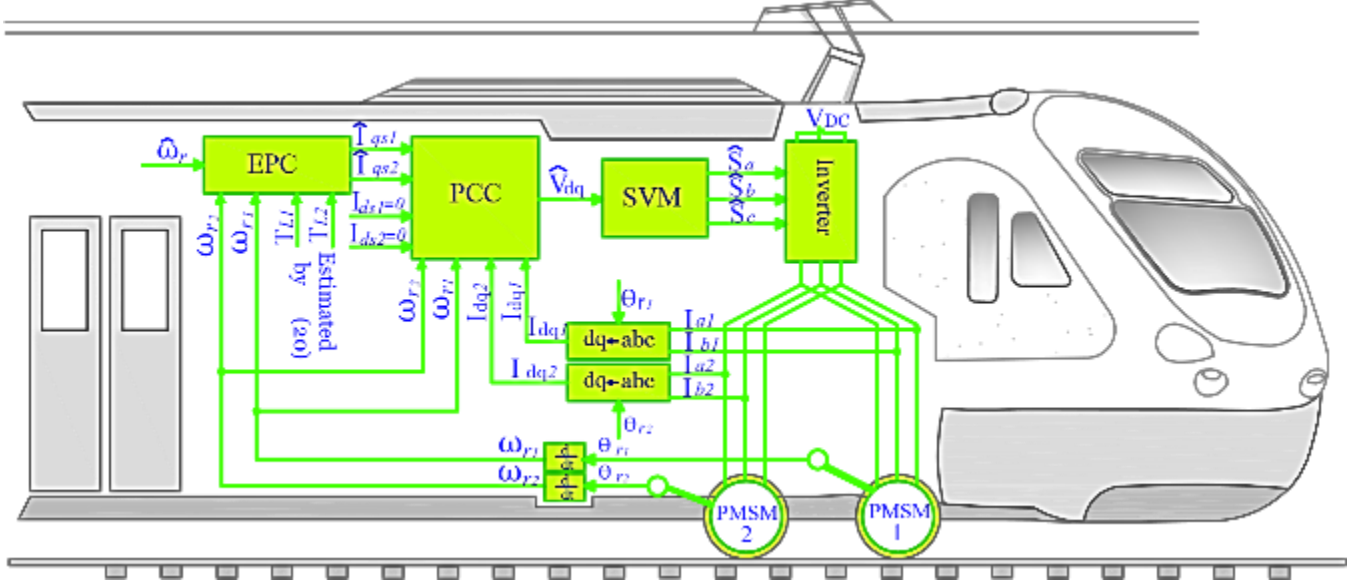
Fig. 1. Block diagram of the proposed method. The EPC block in the outer loop is related to speed control and the PCC block in the inner loop is related to current control.

A. Modelling of two PMSM motors in MIDP system

The PMSM motors have advantages such as high torque density, high efficiency, and low volume. They are preferred in the rail transportation system over other electric motors [32]. Therefore, two identical surface mounted PMSM motors are used in MIDP system, whose electrical equations can be found in the rotor reference frame [33]. The rotor coordinates of the motors do not match when the mechanical load of the motors is not the same for a specific application or for a period. As a result, according to the mechanical load of the motors, the coordinates have different angles. In such cases, the inverter dq coordinate system cannot be matched to the coordinate system of both motors at any time.

The problem can be solved by transferring the governing equations of the second motor to the dq coordinate system of the first motor whereby the inverter dq coordinate system will be matched to the rotor reference frames of both motors. The following coordinate conversion (1) has been employed to transfer the state space equations of the second motor to the rotor reference frame of the first one [34].

$$f_{dqs2}^{r_1} = ({}^{r_2}K_s{}^{r_1})f_{dqs2}^{r_2}; \tag{1}$$
$${}^{r_2}K_s{}^{r_1} = \begin{bmatrix} cos(\theta_{r1} - \theta_{r2}) & -sin(\theta_{r1} - \theta_{r2}) \\ sin(\theta_{r1} - \theta_{r2}) & cos(\theta_{r1} - \theta_{r2}) \end{bmatrix}$$

where $f_{dqs2}^{r_2}$ is the state variable vectors of the second motor in its rotor reference frame and $f_{dqs2}^{r_1}$ is the transferred state variable vectors of the second motor to the rotor reference frame of the first motor, and θ_{r1} and θ_{r2} are the electric angle displacements of the motors, respectively. The electrical equations of the second motor

in the dq coordinate system of the first motor are provided by (1) as follows:

$$\begin{cases} \frac{d}{dt}\left(I_{qs2}^{r_1}(t)\right) = \frac{1}{L}V_{qs2}^{r_1}(t) - \frac{r_s}{L}I_{qs2}^{r_1}(t) - \cdots \\ \dots - \omega_{r1}(t)I_{ds2}^{r_1}(t) - \frac{1}{L}\omega_{r2}(t)\psi_f\,cos(\theta_{r1} - \theta_{r2})\,; \\ \frac{d}{dt}\left(I_{ds2}^{r_1}(t)\right) = \frac{1}{L}V_{ds2}^{r_1}(t) - \frac{r_s}{L}I_{ds2}^{r_1}(t) + \cdots \\ \dots + \omega_{r1}(t)I_{qs2}^{r_1}(t) - \frac{1}{L}\omega_{r2}(t)\psi_f\,sin(\theta_{r1} - \theta_{r2})\,; \end{cases} \tag{2}$$

Where $V_{qs2}^{r_1}(t), I_{ds2}^{r_1}(t), I_{qs2}^{r_1}(t)$ and $V_{ds2}^{r_1}(t)$ are the stator current and voltage of the second motor in the first motor dq coordinate system.

B. Design of the MIDP system Controllers

The control signal generation algorithm based on the Pontryagin's Maximum Principle, which is employed in MPC-based current controller design, are described first.

B.1 Design algorithm of torque component current controller based on Pontryagin's Maximum Principle:

Using Taylor expansion, the nonlinear model of the control system at t_i is defined as:

$$\begin{aligned} X^{\bullet}(t) = f(X(t), U(t), t) &= A(X(t_i), t_i)X(t) + \cdots \\ &+ \cdots B(t_i)U(t) + D(X(t_i), t_i); \\ X_{min} &\le X(t) \le X_{max} \\ U_{min} &\le U(t) \le U_{max} \end{aligned} \tag{3}$$

Where $X(t_i)$ is the state vector at the moment t_i, and A, B and D are the state matrix, input matrix and disturbance matrix, respectively, produced by the linearization and uncontrollable inputs. For the controlled system given in (3), to reach the desired condition, the performance index

of MPC problem is considered as follows:

$$\mathcal{J} = Min\frac{1}{2}\Big[\big(X(t_f) - \hat{X}\big)^T Q_f\big(X(t_f) - \hat{X}\big) + \int_{t_i}^{t_f}\big(X(t) - \hat{X}\big)^T Q\big(X(t) - X^*\big) + U^T(t)RU(t)d\tau\Big];$$

(4)

Where $Q \geq 0, Q_f \geq 0$ and $R > 0$ are weighting matrices to be selected, $\hat{X}$ is the reference state vector, X is the optimal value of the state vector, t_f is the end of the predictive horizon, and $X(t_f)$ is the state vector at t_f. The first statement is the final cost function and the other is the integral cost function. The Pontryagin's Maximization Principle can be used to solve the MPC problem [35]. For this purpose, the Pontryagin function is written as follows:

$$\mathcal{H} = Z\big(X(t), \hat{X}, t\big) + \psi^T(t)\big(f(X(t), U(t), t)\big);$$

(5)

Where $\psi(t)$ is the quasi-variable state vector with equal dimension to the state vector $X(t)$, and $Z(X(t), X^*, t)$ is the second statement of (4). Based on the Pontryagin's Maximum Principle, the necessary optimization conditions are $X^{\bullet}(t) = \frac{\partial \mathcal{H}}{\partial \psi}$, $\psi^{\bullet}(t) = -\frac{\partial \mathcal{H}}{\partial X}$ and $\frac{\partial \mathcal{H}}{\partial U} = 0$. The linear equation of the controlled system and the necessary conditions of optimality make it possible to write the differential equations as follows:

$$\begin{cases} X^{\bullet}(t) = A\big(X(t_i)\big)X(t) - BU(t) + D(X(t_i), t_i); \\ \psi^{\bullet}(t) = -Q\big(X(t) - \hat{X}\big) - A^T\big(X(t_i)\big)\psi(t); \\ U(t) = R^{-1}B^T\psi(t); \\ X(t_i) = X_{t_i}; \\ \psi(t_f) = \left(\frac{\partial\big(X(t_f) - \hat{X}\big)^T Q_f\big(X(t_f) - \hat{X}\big)}{\partial X(t)}\right)_{t_f} = \cdots \\ \qquad\qquad\qquad\qquad \cdots = Q_f\big(X(t_f) - \hat{X}\big); \end{cases}$$

(6)

To calculate the control signals, the forward Euler method is used to approximate the left side of (6).

$$\frac{X(t_i+1) - X(t_i)}{\tau_p} = A\big(X(t_i)\big)X(t) - BR^{-1}B^T\psi(t) + D(X(t_i), t_i);$$

(7)

$$\frac{\psi(t_i+1) - \psi(t_i)}{\tau_p} = -Q\big(X(t) - \hat{X}\big) - A^T\big(X(t_i)\big)\psi(t);$$

(8)

where τ_p is small enough. After simplifying (7) and (8), calculating the predicted value of the state vector at the end of the sampling interval, and also calculating the value of the quasi-state variable at the beginning of the sampling interval, $\psi(t_i)$ can be written as follows:

$$\psi(t_i) = \rho_1 M^{-1}\rho_2 X(t_i) + \rho_1\big((M^{-1}\rho_3\rho_1 - 1)\hat{X} + \tau_p M^{-1}D(X(t_i), t_i)\big);$$

(9)

The calculations related to the coefficients ρ_1, ρ_2, ρ_3 and

M can be found in the appendix. Thus, having $\psi(t_i)$, the control signals are obtained as follows:

$$\begin{cases} U(t_i) = \alpha\big(X(t_i)\big)X(t_i) + \beta\big(X(t_i)\big); \\ \alpha\big(X(t_i)\big) = -R^{-1}B^T\rho_1 M^{-1}\rho_2; \\ \beta\big(X(t_i)\big) = -R^{-1}B^T\rho_1\Big((M^{-1}\rho_3\rho_1 - 1)\hat{X} + \cdots \\ \qquad\qquad\qquad\qquad \cdots + \tau_p M^{-1}D(X(t_i), t_i)\Big) \end{cases}$$

(10)

As it can be seen in (10), the control signals are obtained as linear-parametric relations from the measurable state variables, making online calculations time shorter. This is because $U(t_i)$ can be calculated, having the feedback state vector, $\alpha\big(X(t_i)\big)$ and $\beta\big(X(t_i)\big)$.

Consequently, the algorithm for generating control signals can be staged as follows:

1. Obtaining the Pontryagin H function based on the designed performance index and the linear model of the system.
2. Obtaining the necessary conditions for optimality in accordance with the Pontryagin's Maximum Principle.
3. Discretization of linear equations with the forward Euler approximation and calculating $\psi(t_i)$ considering the boundary conditions.
4. Determining the necessary conditions for controllability, with the assumptions of $t_f = t_i + 1$ and τ_p to be small enough.
5. Achieving equations of control signals analytically, based on predicted state and quasi-state variables.

B.2 Designing current controller in MIDP system with two PMSM motors:

To generate voltage signals in the proposed PCC, the electrical equations of both motors are used in the first motor dq coordinate system. Therefore, the state space model for setting the inner loop controller is as follows:

$$\begin{cases} \begin{bmatrix} I_{qds1}^{r_1}(t) \\ I_{qds2}^{r_1}(t) \end{bmatrix}^{\bullet} = \begin{bmatrix} \gamma_{11} & \gamma_{12} \\ \gamma_{21} & \gamma_{22} \end{bmatrix}\begin{bmatrix} I_{qds1}^{r_1}(t) \\ I_{qds2}^{r_1}(t) \end{bmatrix} + \cdots \\ \qquad \cdots + \frac{1}{L}\begin{bmatrix} 1 & 0 & 1 & 0 \\ 0 & 1 & 0 & 1 \end{bmatrix}^T\begin{bmatrix} V_{qs}^{r_1}(t) \\ V_{ds}^{r_1}(t) \end{bmatrix} + \begin{bmatrix} \Delta_1 \\ \Delta_2 \end{bmatrix}; \\ \gamma_{11} = \gamma_{22} = \begin{bmatrix} -\dfrac{r_s}{L} & -\omega_{r1}(t_i) \\ \omega_{r1}(t_i) & -\dfrac{r_s}{L} \end{bmatrix}; \\ \Delta_1 = \dfrac{\psi_f}{L}\begin{bmatrix} -\omega_{r1}(t_i) \\ 0 \end{bmatrix}; \\ \Delta_2 = \dfrac{\psi_f}{L}\omega_{r2}(t_i)\begin{bmatrix} -\cos\big(\theta_{r1}(t_i) - \theta_{r2}(t_i)\big) \\ -\sin\big(\theta_{r1}(t_i) - \theta_{r2}(t_i)\big) \end{bmatrix}; \end{cases}$$

(11)

where $\gamma_{12} = \gamma_{21}$ is zero-matrix 2×2, and I is a 2×2 identity matrix. Since both motors are fed by a three-phase inverter,

it is not possible to adjust the control variables using four voltage signals. Therefore, it is assumed that $V_{qs1}^{r1} = V_{qs1}^{r1} = V_{qs2}^{r1}$ and $V_{ds}^{r1} = V_{ds1}^{r1} = V_{ds2}^{r1}$. In Equation (11), the variables $\omega_{r1}(t_i)$ and $\omega_{r2}(t_i)$ are the feedback values of the motor speeds, and $\theta_{r1}(t_i)$ and $\theta_{r2}(t_i)$ are the feedback values of the electrical angles at t_i.

Considering the controller design algorithm, the performance index should be determined based on the intended control goal. As a result, for both motors to follow the reference values of currents under unequal mechanical load conditions and at the same time the voltage signals not to exceed the boundary limits, the performance index is defined according to (4). The required vectors and matrices are defined as follow:

$$\begin{cases} X(t) = \begin{bmatrix} I_{qds1}^{r1}(t) & I_{qds2}^{r1}(t) \end{bmatrix}^T; \\ U(t) = \begin{bmatrix} V_{qs}^{r_1}(t) & V_{ds}^{r_1}(t) \end{bmatrix}^T; \\ \hat{X} = \begin{bmatrix} \hat{I}_{qds1}^{r_1}(t) & \hat{I}_{qds2}^{r_1}(t) \end{bmatrix}^T; \\ R = \begin{bmatrix} R_{11} & 0 \\ 0 & R_{22} \end{bmatrix}; \end{cases}$$

and Q and Q_f are deterministic positive diameter 4×4 matrices. It is assumed that $\hat{I}_{ds1} = \hat{I}_{ds2} = 0$, so that the proposed PCC can be adjusted based on the field-oriented control method.

By obtaining the Pontryagin H function and applying the necessary optimization conditions, the first-order state equations are as follows:

$$\begin{bmatrix} I_{qds1}^{r_1}(t) \\ I_{qds2}^{r_1}(t) \end{bmatrix}^{\bullet} = \begin{bmatrix} \gamma_{11} & \gamma_{12} \\ \gamma_{21} & \gamma_{22} \end{bmatrix} \begin{bmatrix} I_{qds1}^{r_1}(t) \\ I_{qds2}^{r_1}(t) \end{bmatrix} -$$
$$\frac{1}{L^2} R^{-1} \begin{bmatrix} 1 & 1 \\ 1 & 1 \end{bmatrix} \begin{bmatrix} \psi_{qds1}(t) \\ \psi_{qds2}(t) \end{bmatrix} - \begin{bmatrix} \Delta_1 \\ \Delta_2 \end{bmatrix}; \quad (12)$$

$$\begin{bmatrix} \psi_{qds1}(t) \\ \psi_{qds2}(t) \end{bmatrix}^{\bullet} = -[Q_{11} \quad Q_{22} \quad Q_{33} \quad Q_{44}] \times I \times$$
$$\left(\begin{bmatrix} I_{qds1}^{r_1}(t) \\ I_{qds2}^{r_1}(t) \end{bmatrix} - \begin{bmatrix} \hat{I}_{qds1}^{r_1}(t) \\ \hat{I}_{qds2}^{r_1}(t) \end{bmatrix} \right) - \begin{bmatrix} \gamma_{11} & \gamma_{12} \\ \gamma_{21} & \gamma_{22} \end{bmatrix} \begin{bmatrix} \psi_{qds1}(t) \\ \psi_{qds2}(t) \end{bmatrix};$$
$$(13)$$

Where I is a 4×4 identity matrix. After applying the forward Euler approximation and simplifications, as well as calculating coefficients $\rho_1, \rho_2, \rho_3, \rho_4$ and M, the control signals are as follows:

$$\begin{bmatrix} V_{qs}^{r_1}(t_i) \\ V_{ds}^{r_1}(t_i) \end{bmatrix} = \begin{bmatrix} F_{11}^{r_1} & F_{12}^{r_1} & F_{13}^{r_1} & F_{14}^{r_1} \\ F_{21}^{r_1} & F_{22}^{r_1} & F_{23}^{r_1} & F_{24}^{r_1} \end{bmatrix} \begin{bmatrix} I_{qds1}^{r_1}(t_i) \\ I_{qds2}^{r_1}(t_i) \end{bmatrix} + \begin{bmatrix} G_{11}^{r_1} \\ G_{21}^{r_1} \end{bmatrix};$$
$$(14)$$

Although each element in matrices F^{r_1} and G^{r_1} has, respectively, 64 and 230 multiplication and 26 and 90 addition operations, the number of mathematical operations is greatly reduced after simplification as multiplication and addition operations for each control signal is 128 and 78, respectively. The reversibility of matrix M should be realized before calculating these matrices. Otherwise, the proposed method would not be efficient. In what follows, the reversibility matrix M is examined.

B.3 The reversibility matrix M:

Calculating the coefficients $\rho_1, \rho_2, \rho_3, \rho_4$ gives the following matrix M:

$$M = \begin{bmatrix} m_{11} + 1 & m_{12} & m_{13} & m_{14} \\ m_{21} & m_{22} + 1 & m_{23} & m_{24} \\ m_{11} & m_{12} & m_{13} + 1 & m_{14} \\ m_{21} & m_{22} & m_{23} & m_{24} + 1 \end{bmatrix}$$

All the elements can be found in the appendix. The weighting values should be $Q_{11} = Q_{33}$, $Q_{22} = Q_{44}$, $Q_{f11} = Q_{f33}$, and $Q_{f22} = Q_{f44}$ must be defined in matrix M. Otherwise, there would be bias in motors. Reversibility is proven when the determinant of M is zero. Determinant of M is as follows:

$$Det(M) = 1 + \left(\frac{1}{\tau_p} - \frac{r_s}{L} \right) \left(\frac{2Q_{f11}}{R_{11}} + \frac{2Q_{f22}}{R_{22}} + \frac{4}{R_{11}R_{22}} (Q_{22}Q_{f11} + Q_{11}Q_{f22}) \left(\frac{\tau_p}{L} \right)^2 + \left(\frac{1}{\tau_p} - \frac{r_s}{L} \right) \frac{4Q_{f11}Q_{f22}}{R_{11}R_{22}} \left(\frac{\tau_p}{L} \right)^2 \right) \left(\frac{\tau_p}{L} \right)^2 + \left(\frac{2Q_{11}}{R_{11}} + \frac{2Q_{22}}{R_{22}} + \frac{4Q_{11}Q_{22}}{R_{11}R_{22}} \left(\frac{\tau_p}{L} \right)^2 \right) \left(\frac{\tau_p}{L} \right)^2; \quad (15)$$

when the value of $\left(\frac{1}{\tau_p} - \frac{r_s}{L} \right)$ is chosen positive, the determinant of matrix M will be non-zero.

In the above approximation, it is assumed that the value of τ_p is smaller than the electrical time constant of the motors. Thus, the determinant of M is always non-zero.

C. MPC-based speed controller design

With the least fluctuation and in the shortest possible time, the motor speeds reach the reference speed when the designed speed controller adjusts the commands of the current-torque components in the inner loop. Accordingly, the performance index is defined as follows:

$$\begin{cases} \mathcal{J} = \min_X \left\{ \frac{1}{2} \int_{t_i}^{t_f} V(\hat{X}, X(\tau), \tau) d\tau \right\} \\ V = \left(\hat{X} - X(t) \right)^T Q_{sw}(t) \left(\hat{X} - X(t) \right) \end{cases}$$
$$(16)$$

Where the state vector $X(t) = [\omega_{r_1}^{\bullet}(t) \quad \xi_{k_1}(t) \quad \omega_{r_2}^{\bullet}(t) \quad \xi_{k_2}(t)]^T$ contains the angular accelerations ($\omega_r^{\bullet}(t)$) and kinetic energies ($\xi_k(t)$). The element values of reference vector are $\begin{bmatrix} 0 & \frac{1}{2}J_t \left(\hat{\omega}_{r_1}(t) \right)^2 & 0 & \frac{1}{2}J_t \left(\hat{\omega}_{r_2}(t) \right)^2 \end{bmatrix}^T$. The total inertia moment of load and motor is J_t, and $Q_{sw}(t)$ is the deterministic positive weighting matrix. Since motors are not mechanically coupled, therefore, the elements associated with their coupling will be zero in the $Q_{sw}(t)$ matrix. By replacing the state and reference

vectors in performance index and minimizing the integral cost function relative to the motor speed slopes, (17) is obtained.

$$\begin{cases} \dot{\omega}_{r_1}(t) = K_{\omega_{r_1}}\left(\left(\hat{\omega}_{r_1}\right)^2 - \left(\omega_{r_1}(t_i)\right)^2\right); \\ K_{\omega_{r_1}} = \frac{2J_t}{p^2}\left(\frac{Q_{sw12}(t)+Q_{sw21}(t)}{Q_{sw11}}\right); \\ \dot{\omega}_{r_2}(t) = K_{\omega_{r_2}}\left(\left(\hat{\omega}_{r_2}\right)^2 - \left(\omega_{r_2}(t_i)\right)^2\right); \\ K_{\omega_{r_2}} = \frac{2J_t}{p^2}\left(\frac{Q_{sw34}(t)+Q_{sw43}(t)}{Q_{sw33}}\right); \end{cases}$$

(17)

The reference and electrical angular speeds of the motors at t_i are $\hat{\omega}_{r_1}, \hat{\omega}_{r_2}, \omega_{r_1}(t_i), \omega_{r_2}(t_i)$, respectively. By choosing $Q_{sw11} = Q_{sw33} = \frac{2}{p}\Delta t^2$ and $Q_{sw12}(t) = Q_{sw21}(t) = \frac{1}{2T_{L_1}(t_i)}$ and also $Q_{sw34}(t) = Q_{sw43}(t) = \frac{1}{2T_{L_2}(t_i)}$ and by choosing an arbitrary value for Q_{sw22} and Q_{sw44}, to keep the matrix $Q_{sw}(t)$ as positive deterministic, (17) is as follows:

$$\frac{2}{p}\dot{\omega}_{r_k}(t)T_{L_k}(t_i)\Delta t^2 = \frac{2J_t}{p^2}\left(\left(\hat{\omega}_{r_k}\right)^2 - \left(\omega_{r_k}(t_i)\right)^2\right);$$

(18)

Where $T_{L_k}(t_i)$ is the load-torque of the kth motor at t_i. If the Δt is small enough, the left side of equation (18) could be approximated as follows:

$$\frac{2}{p}\dot{\omega}_{r_k}(t)T_{L_k}(t_i)\Delta t^2 = \frac{2}{p}\frac{\Delta\omega_{r_k}(t)}{\Delta t}T_{L_k}(t_i)\Delta t^2 = \frac{2}{p}\Delta\omega_{r_k}(t)T_{L_k}(t_i)\Delta t$$

Since $\Delta\omega_{r_k}(t)T_{L_k}(t_i) = \Delta P_k(t)$, the equation (18) is the power in electric motor shaft in Δt period. Therefore, the left side of the equation (18) would be looked like this.

$$\frac{2}{p}\dot{\omega}_{r_k}(t)T_{L_k}(t_i)\Delta t^2 = \frac{2}{p}\Delta P_k(t)\Delta t = \frac{2}{p}\Delta E_k(t)$$

where $\Delta E_k(t)$ is the flow energy to the motor at a definite time. It should be noted, the T_{L_k} has been assumed a constant parameter in Δt period. The right side of (18) is the difference of the kinetic energy. The $\frac{2J_t}{p^2}\left(\omega_{r_k}(t_i)\right)^2$ is the kinetic energy in the motor shaft, and the $\frac{2J_t}{p^2}\left(\hat{\omega}_{r_k}\right)^2$ is the kinetic energy in the reference speed.

Using the mechanical equation of PMSM motors, the commands of stator current-torque components are as follows:

$$I_{qsk}^{r_1}(t_i) = \frac{8J\cdot J_t}{\Delta t^2 3p\psi_f T_{L_k}(t_i)}\left(\left(\hat{\omega}_{r_k}\right)^2 - \left(\omega_{r_k}(t_i)\right)^2\right) + \frac{8B_m}{3p^2\psi_f}\omega_{r_k}(t_i) + \frac{4}{3p\psi_f}T_{L_k}(t_i); \quad (19)$$

Where k = 1, 2. Since the balance between the required energy and the kinetic energy on the motor shaft play an important role in the generation of control signals, this method of speed control can be introduced

as Energy-based Predictive Control (EPC). When the $\hat{\omega}_{r_k}$ is issued, the kinetic energy difference appears. If the energy flowing to the motor shaft is greater than the kinetic energy difference, the motor reaches a speed more than the reference speed in transient mode, and vice versa. If the energy delivered to the motor is equal to the kinetic energy difference, no excess energy will be injected into the motor. Therefore, the energy that causes the speed fluctuations will not inject into the motor. When the motor speed approaches the reference speed, the kinetic energy difference will be reduced, and the energy delivered to the motor for the desired changes is reduced. Equation (19) suggests when the speed changes of each motor are at such a way that each of the commands $\hat{I}_{qs1}^{r_1}(t_i)$ and $\hat{I}_{qs2}^{r_1}(t_i)$ exceeds the nominal current limits, the value of the nominal current of the motors must replace the calculated command. It is necessary to mention that this controller can use in any electrical smooth pole motor.

D. Load torque calculation:

Since (19) spends on the load torque, T_L needs to be available to set the command value $I_{qs}^{r_1}$. The load torque is usually measured by a torque meter or is calculated using estimation methods. Since a torque meter increases the cost and the measurement noise of electric propulsion, computational methods are used to estimate the amount of load torque. Considering the mechanical equation and the electromagnetic torque equation of the surface mounted PMSM motor, the load torque equation can be written using the backward Euler approximation, as follows:

$$T_L(t_i) = \frac{3}{2}\frac{p}{2}\psi_f I_{qs}^r(t_i) - J\frac{2}{p}\left(\frac{\omega_r(t_i)-\omega_r(t_{i-1})}{\tau_p}\right) - B_m\frac{2}{p}\omega_r(t); \quad (20)$$

To increase the accuracy of the calculated value, the value of load torque is set equal to the average of the last 10 samples.

E. Impact of constraints on MIDP system drive with two PMSM motors:

It is possible to use the electrical and mechanical equations of motors in equation (6). In this case, the speed and current controllers will be integrated. If, in MIDP, the MPC speed and current controllers were integrated, two control signals $V_{ds}^{r_1}$ and $V_{qs}^{r_1}$ would control six state variables $I_{ds_{1,2}}, I_{qs_{1,2}}$ and $\omega_{r_{1,2}}$. Doing so would involve two important drawbacks. First, controlling six control variables with two control signals would be challenging. Second, the control signals $V_{ds}^{r_1}$ and $V_{qs}^{r_1}$ highly depend on the motor speeds and a change in the speed command would cause many changes in them. Therefore, it would increase the possibility that voltages are limited by constraints by changing the speed

command. This would cause the motor control process to deviate from the optimal mode path. In this paper, an external loop controller is introduced.

One of its features is that it determines the optimal I_{qs} current commands in proportion to the speed command changes. That is, in a sampling interval, the total kinetic energy needed to change the motor speeds is calculated and the speed slope of each motor is determined, which is based on a portion of the total kinetic energy applicable to it.

Another feature of the controller is the optimal determination of the speed slope based on the selected cost function, which causes the final value of the motor speeds to be reached in a short interval. If the calculated speed slope does not lead to the set value in the short interval, the nominal limits of the currents are selected. This means the full capacity of the motors is used. In other words, the kinetic energy of each motor is taken into account in calculating the speed slope of that motor, and, consequently, the excess energy is not imposed on them and speed fluctuation decreases significantly.

III. SIMULATION RESULTS

To show the performance and capability of the proposed controller, MATLAB / Simulink software is used to run the proposed drive technique. Because low-inertia motors have fast dynamics, selecting such a motor can be a major challenge for controllers to generate control signals. Since the controller performance was very good in low inertia motors, proper performance is not far from expectation in high inertia motors.

Hence, two identical PMSM motors manufactured by LS Company with XML-SB04A series are chosen as MIDP system motors. The specifications are listed in Table 1.

Table 1
PMSM motor parameters

Motor Parameter		Parameter Value
Nominal Power	P_{rate}	400^{Watt}
Nominal Current	I_{rate}	2.89^{A}
Pole Number	p	8
Stator Resistance	r_s	0.82^{Ω}
Stator Inductance	L	3.66^{mH}
Permanent Magnet Flux	ψ_f	0.0734^{wb}
Nominal Speed	N_{syn}	$3000^{r.p.m}$
Nominal Torque	T_{rate}	$1.27^{N.m}$
Maximum Torque	T_{max}	$3.82^{N.m}$
Moment of Inertia	J	0.0321×10^{-4} $^{Kg.m^2}$
Friction Coefficient	B_m	0.6×10^{-6} $^{N.m.Sec}$

Table 2
Three-phase inverter parameters

Inverter Parameter		Parameter Value
DC Power Supply	V_{DC}	173^{V}
Switching Frequency	f_{SW}	8^{KHz}
On-Mode Resistance of Power Switches	$R_{DS(on)}$	0.019^{Ω}

The specifications of the SVM modulation inverter are listed in Table 2. Based on section II, the internal and external loop controller values should be determined. In the design of the inner loop controller, the value $\tau_p = 0.125 \times 10^{-3}$ and the weighting matrices are selected as follows:

$$R = \begin{bmatrix} 1 & 0 \\ 0 & 1 \end{bmatrix}; \quad Q = \begin{bmatrix} 15 & 0 & 0 & 0 \\ 0 & 85 & 0 & 0 \\ 0 & 0 & 15 & 0 \\ 0 & 0 & 0 & 85 \end{bmatrix};$$

$$Q_f = \begin{bmatrix} 280 & 0 & 0 & 0 \\ 0 & 5800 & 0 & 0 \\ 0 & 0 & 280 & 0 \\ 0 & 0 & 0 & 5800 \end{bmatrix};$$

In EPC speed controller, $\Delta t = 0.0118$. The sampling frequency of the motor feedback currents is assumed to be 25^{KHz}. In this paper, to evaluate the validity of the control method, the results are compared with the ICS-MPC method. In this method, the amplitude and the angle of the voltage vector are incrementally increased by 1% and 1 degree, respectively. For each step, the discrete electrical equations of the PMSM motors are solved and the values of the state variables (I_{dqs}) are determined. Then, the error rate of the state variables is calculated by the square cost function in (21).

$$CF = Min \sum_{j=1}^{2} \left[K_{\psi_j} \left| \hat{I}_{ds_j} - I_{ds_j}^{r_1} \right|^2 + K_{T_j} \left| \hat{I}_{qs_j} - I_{qs_j}^{r_1} \right|^2 \right]; \quad (21)$$

Where $\hat{I}_{dqs}$ are the reference control signals obtained from (19). Finally, by calculating the cost function 36,000 times in a sample time, the voltage vector leading to the lowest cost function is selected. Although having the time for this huge amount of calculation in microcontroller is not feasible, the comprehensive optimal value of the cost function can be achieved by searching the entire space vector of the control signal.

Fig. 2 provides a basis to compare the performance of the introduced method with the ICS-MPC method with $K_{\psi_j} = 0.1$ and $K_{T_j} = 1.1$. The used control strategy in Fig. 2 is such that the motors are started with nominal load torque, and in t=0.05 the load torque of the second motor is suddenly reduced by 30%. Then, the speed of the motors is simultaneously reduced by 50% under unequal load torques at t=0.1. At last, the reduced load torque of the second motor and the speed command change to their nominal values at t = 0.2. It can be seen that both methods have similar responses. However, the amount of calculations in ICS-MPC in each cycle is significantly higher than the proposed method. Thus, according to (14) and (19), the proposed method has a more prompt and accurate control over motors. Additionally, it needs a cheaper microcontroller.

For a more accurate comparison, Table 3 shows the THD and Integral Square Error (ISE) values in both motors at different speeds. The ISE is obtained by the following equation:
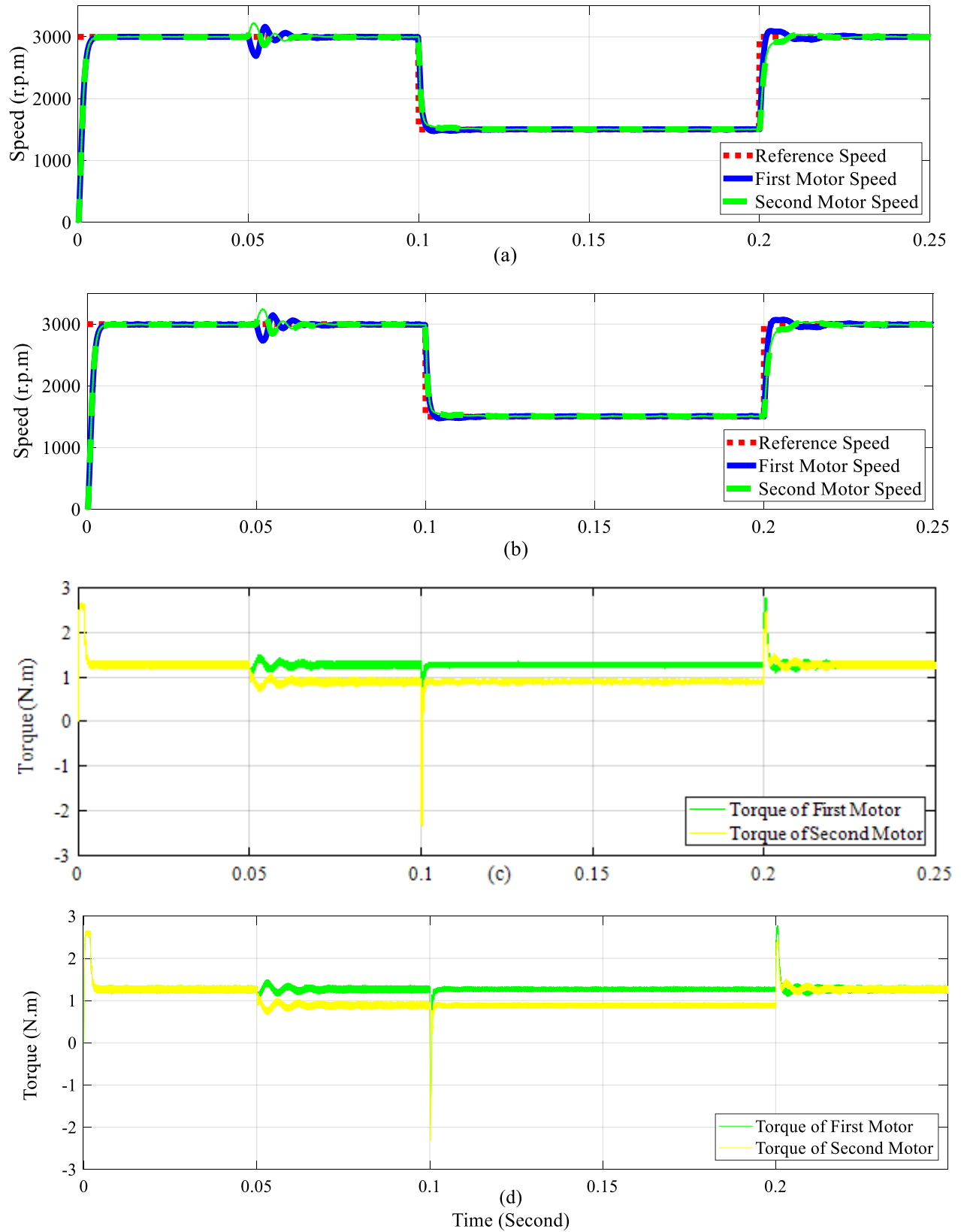
Fig. 2. The speeds and torques of PMSM motors. (a) Speeds and (b) torques of motors in the proposed method. (c) Speeds and (d) torques of motors in the ICS-MPC method.

$$ISE = \sum_{k=1}^{2}\left(\hat{\omega}_{r,k} - \omega_{r,k}\right)^2 \Delta t; \qquad (22)$$

Table 3
Comparison of THD and ISE value in the proposed MPC and ICS-MPC methods.

speed (rpm)	MPC Proposed			ICS-MPC		
	THD 1st Motor	THD 2nd Motor	ISE	THD 1st Motor	THD 2nd Motor	ISE
1500	1.87	1.37	0.1152	2.0	1.47	0.1617
3000	2.27	1.58	0.1381	2.31	1.60	0.1946

A. Load torque changing at an equal speed of motors

In what follows, the performance of the FCS-MPC method and the proposed method are compared in three different control strategies. The internal loop control coefficients of FCS-MPC and ICS-MPC methods are the same. In the outer loop, PI controllers are used. Fig. 3 displays the speeds and torques of the motors in the FCS-MPC and the proposed methods in three strategies.

The different performances of these two methods can be seen by comparing the plots. Moreover, the waveform of speeds in each strategy is magnified in Fig. 4.

In this strategy, the motors have equal nominal speeds and load torques in startup. In 0.05 second, the 2nd motor load is abruptly reduced by 30% and lasts till 0.1 second. As shown in Fig. 4d, the controller's goal during this strategy is only to perform the 2nd motor torque command and has no

control over the 1st motor in transient conditions. That is, simultaneous control of two motors has not been realized. On the other hand, the speed of the 2nd motor shown in green in Fig. 4d is well controlled, while the speed of the 1st motor shown in blue in Fig. 4d indicates that there is no control over the first motor in the same period. This lack of control causes the first motor speed to deviate more than 400 rpm from the reference speed, and the produced undershoot in the speed waveform can cause tension, strain, and motor shaft fatigue. As a result, the performance of the FCS-MPC method indicates that it could control one of the motors in transient conditions, and the other one could not be controlled. However, both motors are controlled simultaneously in the proposed method at any point in time (Fig. 4a).

As can be seen in Fig. 4a, in the time of 0.075 second, the speeds of the two motors are equal and approach the reference value with a slight difference. However, in the meantime, the speeds of motors are in fluctuation (Fig. 4d), which appears as a disturbance in motor torque (Fig. 3d).

As a result, the proposed method achieves faster the steady-state condition than the FCS-MSC method. Furthermore, the low accuracy of the FCS-MPC method has caused constant fluctuations in the motor torque waveform, and consequently distortion in motor current (Fig. 5c and Fig. 5d).
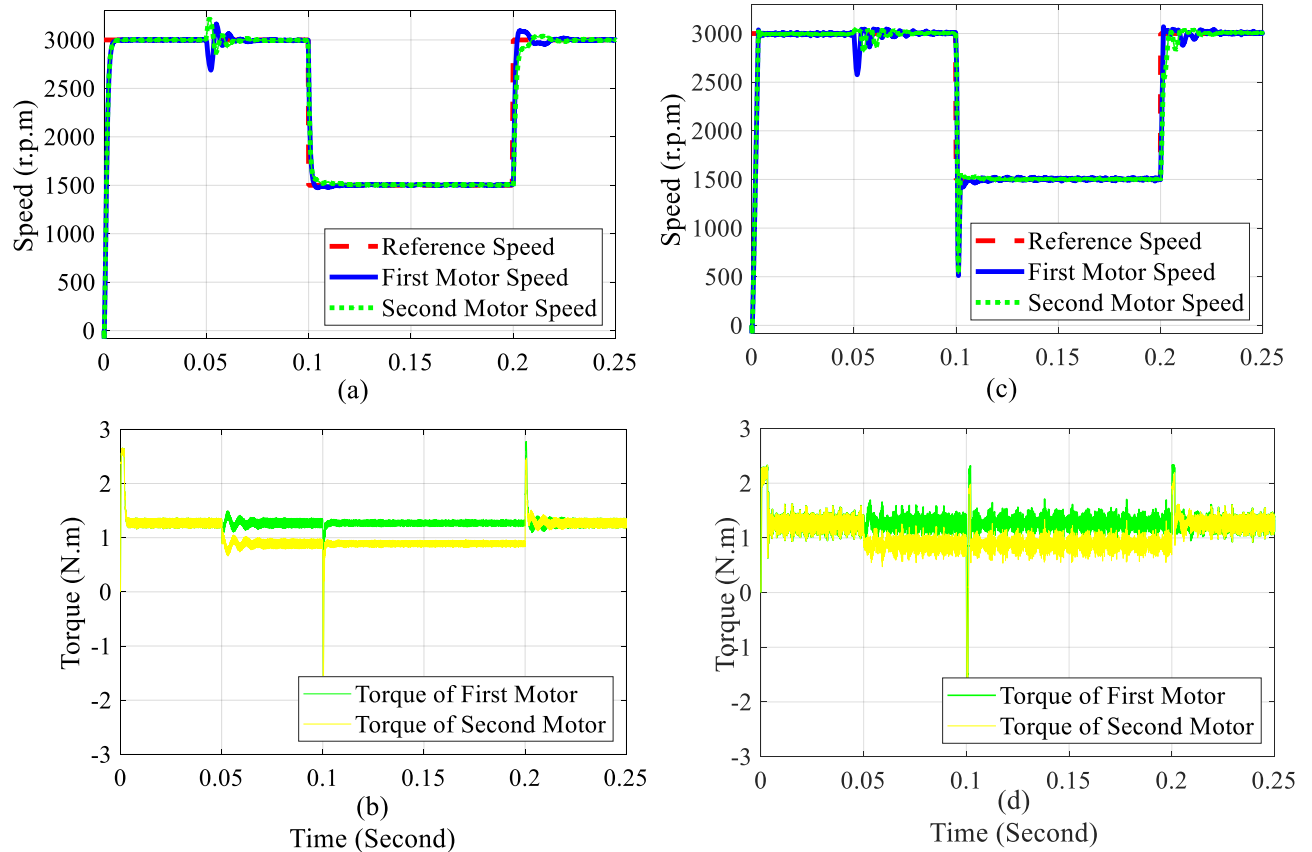

Fig. 3. The speeds and torques of PMSM motors. (a) Speeds and (b) torques of motors in the proposed method. (c) Speeds and (d) torques of motors in the FCS-MPC method.
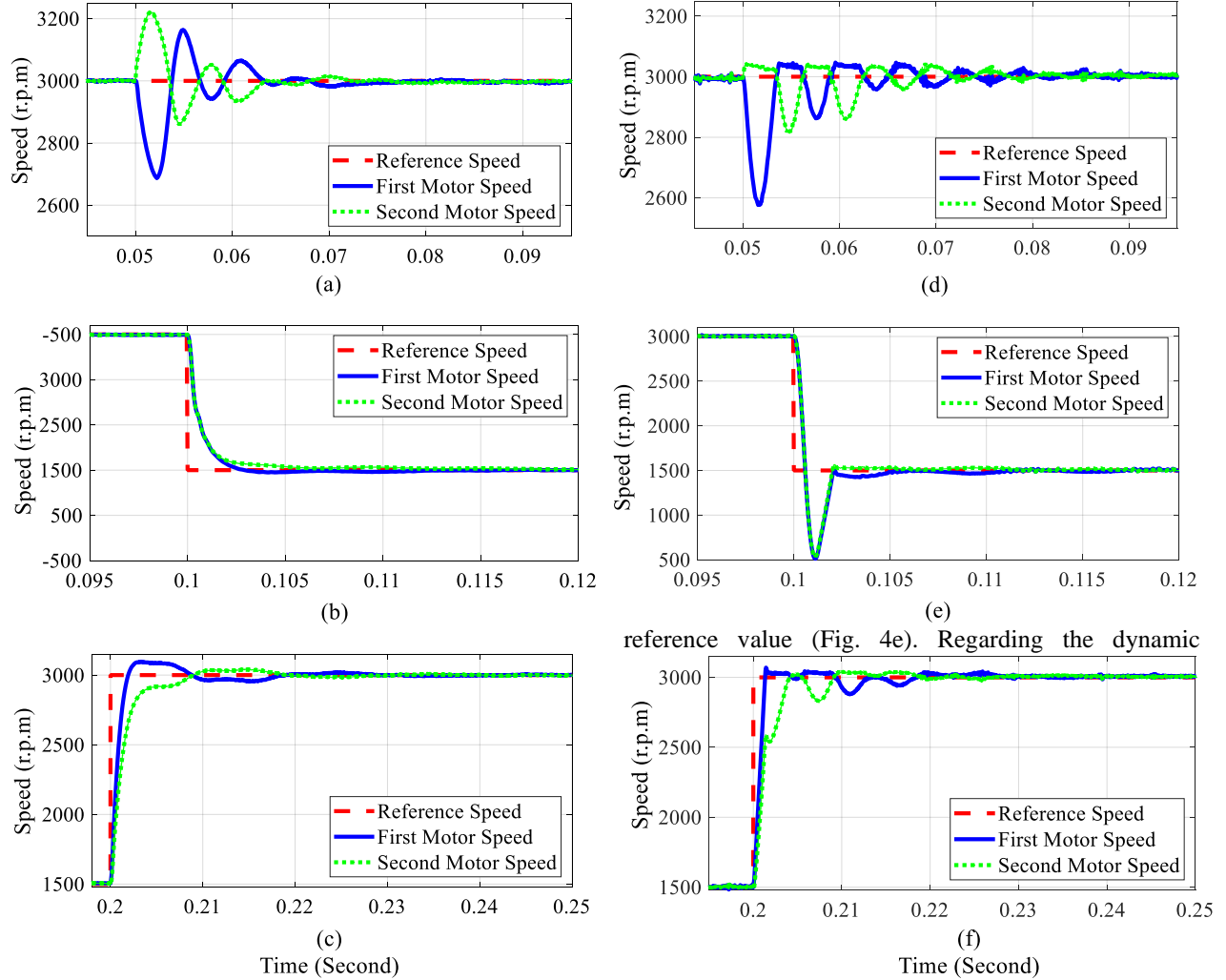
Fig. 4. Magnified plots of the MIDP system speeds. (a-c) Speed motors in the proposed method. (d-f) Speed motors in the FCS-MPC methods.

However, it is not present in Fig. 5a and Fig. 5b waveforms. In addition, the motor currents become in phase in less than 0.02 second, but the currents in the FCS-MPC method have phase differences for a longer period.

B. Simultaneous change of motor speeds at unequal load torques:

In this strategy, the motors have unequal load torques, and their speed command is changed in steps at a rate of 50% of the nominal value in 0.1 second until 0.2 second. To achieve the deceleration, braking torque is applied.

The braking torque is continuously increased to reduce the speed of the motors in the FCS-MPC method. When the motor speeds reach the reference value, the electromagnetic torque of the motors is much lower than the load torque, and the negative acceleration reaches its maximum value. When controllers act this way, the motor speeds have a 1000 rpm deviation from the reference value (Fig. 4e). Regarding the dynamic performance of FCS-MPC controllers within the interval, the transient state fluctuations can be attributed to the excess energy imposed on motors. However, in the proposed method, the new reference speed value is taken into account in the prediction horizon of the external loop controller. Therefore, from the very beginning, it applies the required braking torque to the motors, and the amount of braking torque decreases as the motor speeds approach the reference value. Consequently, no excess energy is applied to two motor shafts.

As shown in Fig. 4b, when the speed decreases, the braking torque also decreases. Similarly, when the electromagnetic torques are equal to the load torques, the motor speeds reach the reference value with no fluctuation in current waveforms (Fig. 5a and Fig. 5b). The controller behaves such that the transient state passes and reaches a stable value without any fluctuations in speed, torque, and current.
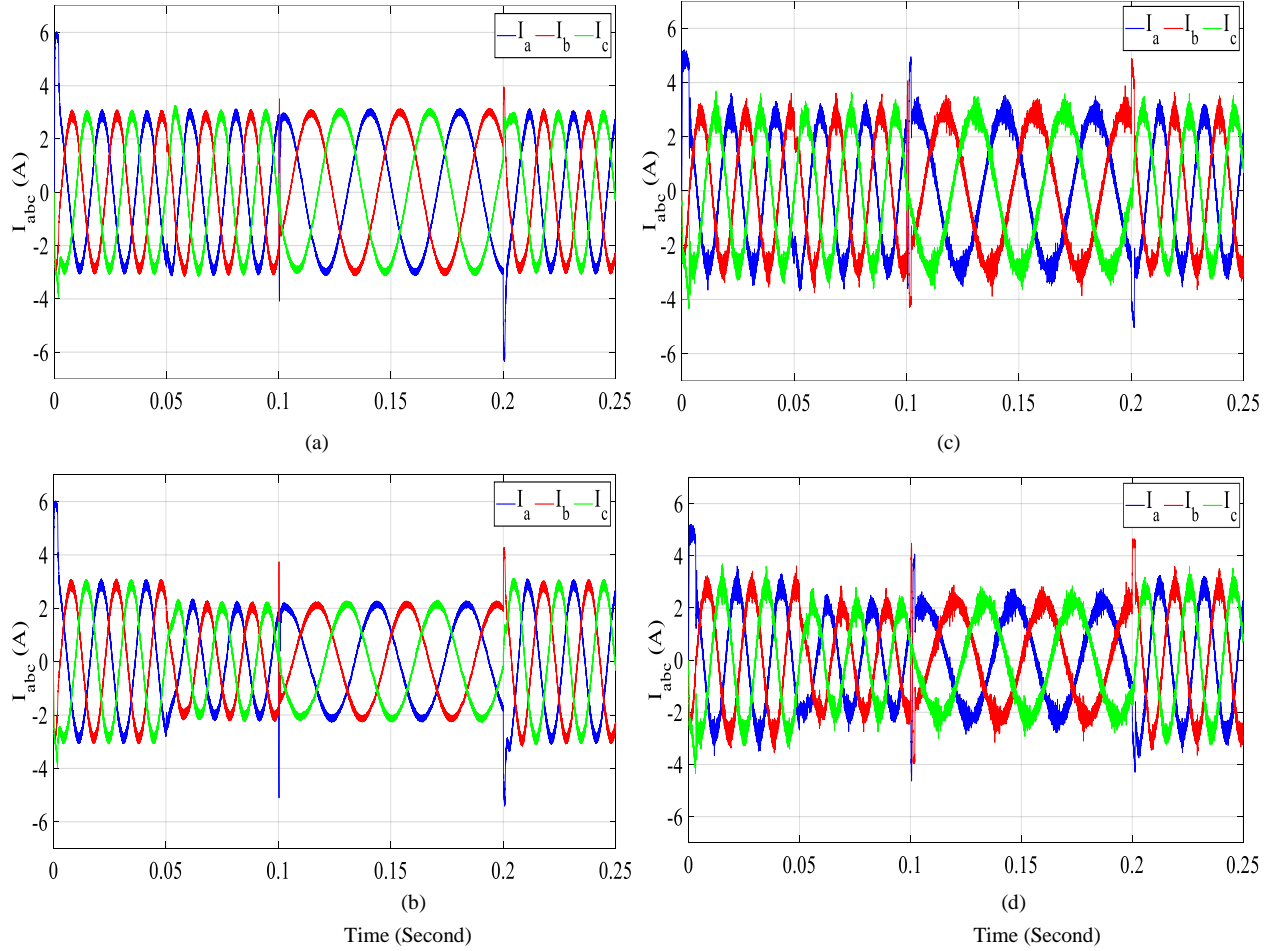
Fig. 5. Three phase currents in both motors. (a) and (b) are currents of 1st and 2nd motor in the proposed method, respectively. (c) and (d) are currents of 1st and 2nd motor in the FCS-MPC method, respectively

C. Simultaneous change of motor speeds and load torques

Within the time interval of 0.2 to 0.25 second, the motor speeds suddenly reach the reference value, and the mechanical load of the 2nd motor returns to the nominal value. In the FSC-MPC method, more control processing is allocated to reducing the difference between motor torque and reference torque regardless of motion dynamics.

This limits the control signals to predetermined constraints (Fig. 4f). However, in the proposed method, by fine-tuning the controllers, a better dynamic performance of the motors is observed without the currents reaching the above constraints (Fig. 4c).

In order to compare the transient performance of two methods, load torque in the 2nd motor is suddenly decreased in three stages. Then, the amount of maximum speed deviations from the reference speed is obtained (Table 4).

Table 5, by investigating the ISE in two different load

torque modes, compares the steady-state performance of the two methods. It shows that the steady-state performance of the designed controller, compared with FCS-MPC method, has less distortion at nominal speed. The results indicate that when MIDP system is driven using the proposed MPC method, it is approximately 568 times and 1.16 times less time consuming than the ICS-MPC and FCS-MPC method, respectively (Table 6).

The saved time frees microcontroller capacity to perform position and speed sensorless control. Table 7 compares the number of mathematical operations for generating voltage signals in the proposed method and the FCS-MPC method.

It is observed that the number of mathematical operations of the conventional FCS-MPC method is somewhat more than the proposed method. In addition, in this method, the minimum value of the objective function must be interpolated. Although the conventional FCS-MPC method is known to have a short computation time, it has more computational time than the proposed method.

Table 4
Comparison of maximum motor speed deviations

$\widehat{\omega}_r$	ΔT_{L_2}	Motor No	Max. Speed Deviation in Proposed MPC	Max. Speed Deviation in FCS-MPC
1500	10%	M_1	82.022	129.430
		M_2	72.536	37.169
	30%	M_1	237.009	425.206
		M_2	218.011	152.425
	50%	M_1	434.911	720.896
		M_2	339.474	279.841
3000	10%	M_1	76.770	124.908
		M_2	76.712	43.056
	30%	M_1	236.174	419.737
		M_2	218.290	184.999
	50%	M_1	428.748	718.076
		M_2	351.419	334.451

Table 5
Comparison of ISEs.

Speed	Load Torque	Motor No	ISE Proposed MPC	FCS-MPC
3000	$T_{L_1} = T_{L_2}$	M_1	0.0179	0.2449
		M_2	0.0179	0.2449
	$T_{L_1} \neq T_{L_2}$	M_1	0.0504	0.2560
		M_2	0.0311	0.2563

Table 6
Elapsed time to produce control signals in the proposed method, FCS-MPC and ICS-MPC.

	Proposed MPC	FCS-MPC	ICS-MPC
Elapsed time	0.004579^{ms}	0.005333^{ms}	2.601221^{ms}

Table 7
Comparison of the number of mathematical operations in two methods.

	Multiplication operations	Addition operations
Proposed Method	257	157
FCS-MPC Method	342	168

D. The sensitivity analysis of the proposed control method

The parameters of two electrical motors produced by the same manufacturer sometimes are different because of temperature effects, operating conditions, and even low-quality production. Therefore, in Fig. 6, the variation effect of the stator resistor, inductance, and linkage flux has been considered on the performance of the designed controllers. To study sensitivity, both motors are rotated at rated speed, and the load torques of the first and second motors are at their rated value and 70 percent rated value, respectively.

The r_s, L and ψ_f values of the first motor are changed step by step from -%20 to +%20 of their rated values in 0.1 seconds while the electrical parameter values of the

second motor are according to Table 1. As seen from Fig. 6(a) to 6(d), undesirable variation in the r_s and L of the first motor at the specified range has been little effect on the speed waveform of both motors in the transient state, and their effects are completely eliminated in the steady state. The effect of the flux variation is shown in Fig. 6(e) and 6(f). Although the ψ_f variation, especially at $\pm 20\%$, has been caused a sharp fluctuation in the transient state, such a linkage flux variation often does not occur in only one of the motors. However, the proposed method is able to maintain the stability of the MIDP motors in steady-state. As a result, undesirable variations in the electrical parameters of the motors do not affect the steady-state performance of the proposed method. The sensitivity of the designed controllers has also been very little to variations in the resistance and inductance of the stator so that significant fluctuations do not observe in the transient state.

E. Comparing both method performances in high-power motors

Since the proposed method should be used to drive the power train, the controllers performance should be checked in the high-power motors. Therefore, two identical surface-mounted PMSM motors are considered, and their specifications are listed in Table 8. The DC-link voltage and switching frequency of the inverter are $600^V, 8^{KHz}$ respectively. The elements of the weighting matrices and the cost function coefficients are as follows:

Table 8
PMSM motor parameters

Motor Parameter		Parameter Value
Nominal Power	P_{rate}	125^{KWatt}
Pole Number	p	8
Stator Resistance	r_s	0.02^{Ω}
Stator Inductance	L	1.0^{mH}
Permanent Magnet Flux	ψ_f	0.892^{wb}
Nominal Speed	N_{syn}	$2000^{r.p.m}$
Nominal Torque	T_{rate}	$600^{N.m}$
Maximum Torque	T_{max}	$1800^{N.m}$
Moment of Inertia	J	$1.57^{Kg.m^2}$

$$Q_{f1} = Q_{f3} = 1200; \quad Q_{f2} = Q_{f4} = 150;$$
$$Q_1 = Q_3 = 125; \quad Q_{f2} = Q_{f4} = 85;$$
$$K_{\psi_j} = 0.3; \quad K_{T_j} = 2.34$$

The control strategy consists of three stages. Both motors start with the nominal load torques at rated speed. In time 0.3 seconds, the load torque of the second motor is abruptly reduced from $600^{N.m}$ to $420^{N.m}$. In the following, the speed command is decreased by step in 1.0 seconds, while motors are in unequal load torque conditions.

As can be seen, no fluctuation observes in the speed and torque waveforms at the start-up and deceleration
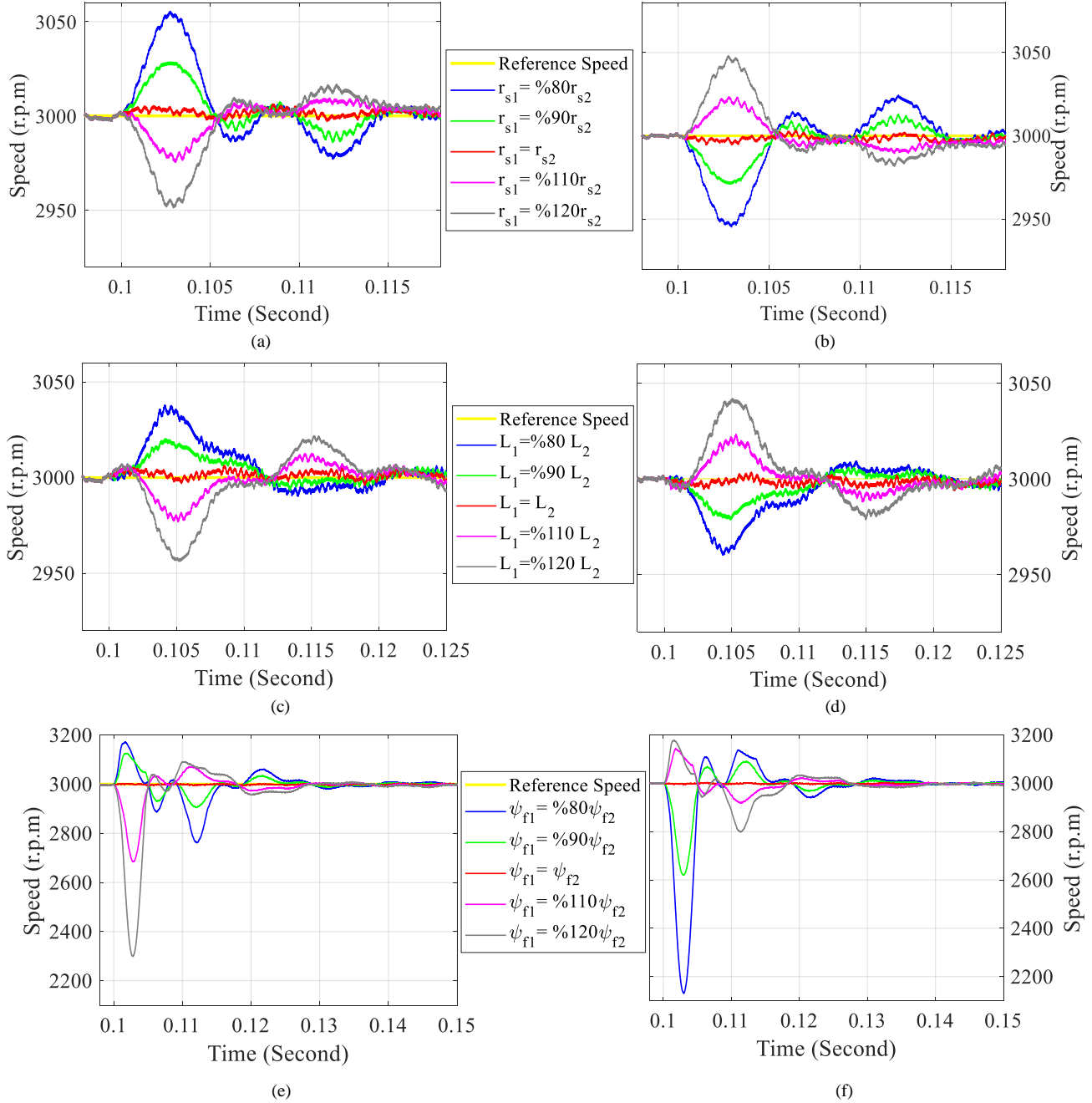
Fig. 6. The effect of the electrical parameter variations over the speed of the motors. (a), (b) The r_{s1} variation on the speed waveform of the first and second motors, respectively. (c), (d) The L_1 variation on the speed waveform of the first and second motors, respectively. (e), (f) The ψ_{f1} variation on the speed waveform of the first and second motors, respectively.

stages, and there is an insignificant fluctuation in the speed and torque waveforms at unbalancing load torque.

As a result, the proposed method has properly controlled both electrical motors in the transient and steady states (Fig.7). The FCS-MPC has also controlled both electrical motors. However, the speed and torque fluctuations can be seen even in the steady-state (Fig.8). The main factors that caused the fluctuations can be found in the controllers of the FCS-MPC. Indeed, the current controller evaluates the cost function (21) with

the limited number of voltage vectors ($V_0, V_1, V_2, ..., V_6$) and selects one of them as the control signal. Therefore, the whole vector space does not evaluate at the cost function, and the optimal control signal does not obtain.

On the other hand, the speed controller coefficients are adjusted only for an operating point. Therefore, the controller does not know how much energy must exchange in unforeseen changes. As a result, the unknown duration should elapse to reduce the produced fluctuations.
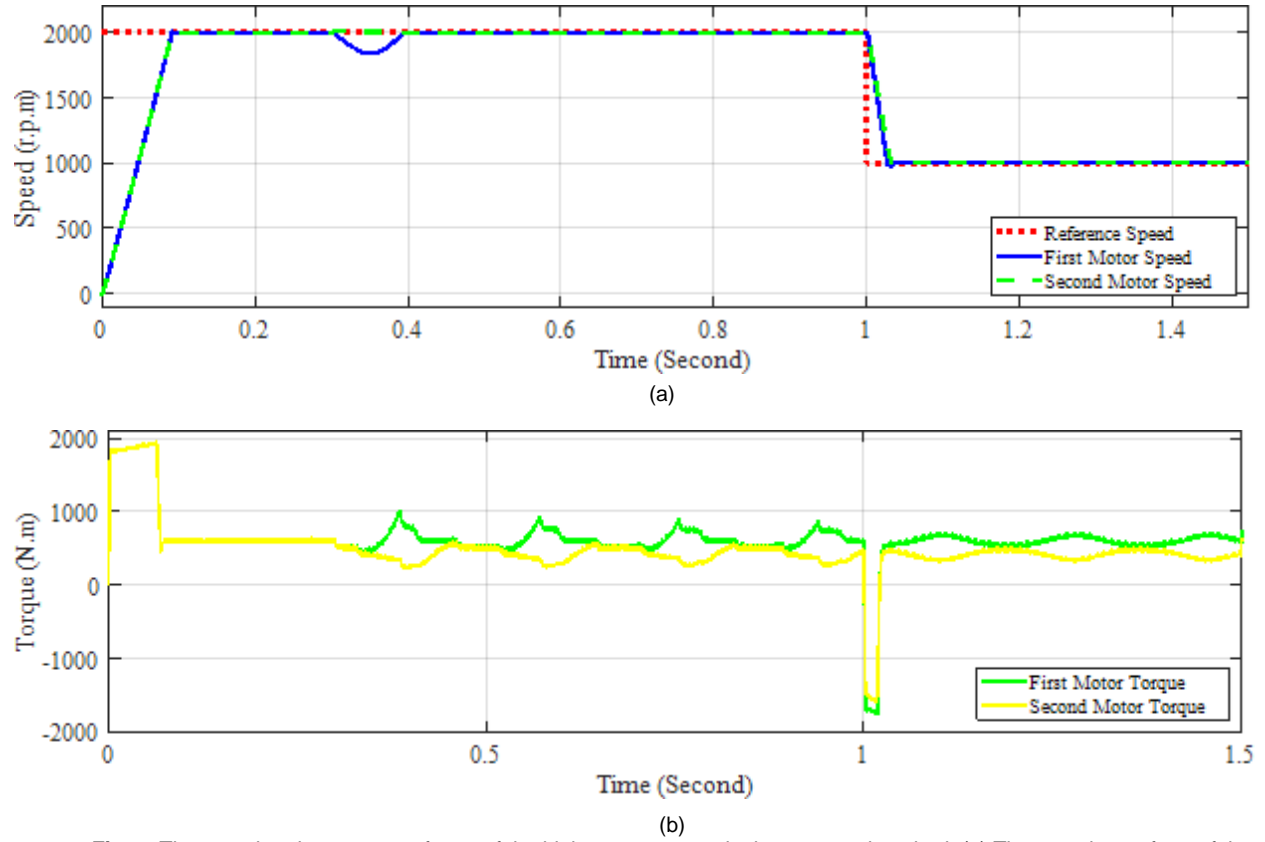
(a)

(b)

Fig. 7. The speed and torque waveforms of the high-power motors in the proposed method. (a) The speed waveform of the reference and both motors. (b)) The torque waveform of both motors.
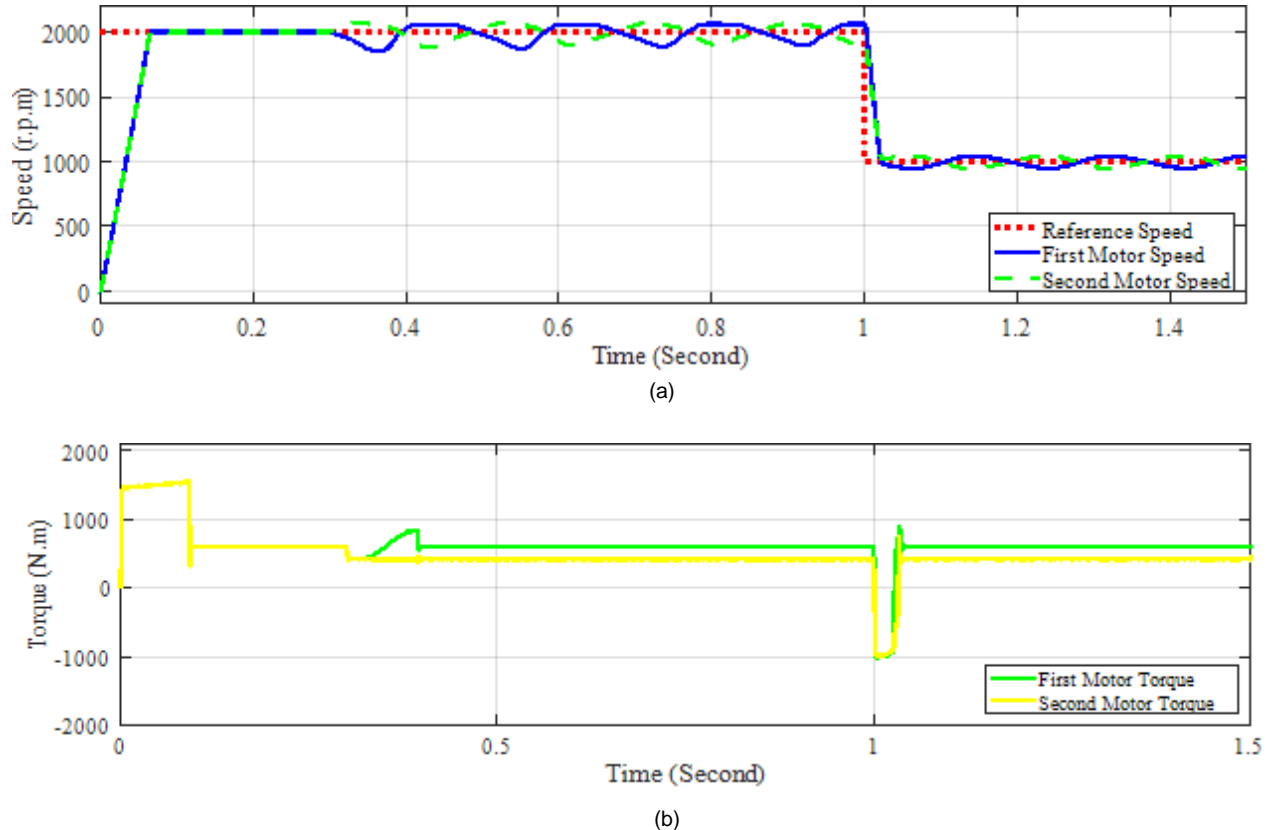

(a)

(b)

Fig. 8. The speed and torque waveforms of the high-power motors in the current FCS-MPC method. (a) The speed waveform of the reference and both motors. (b) The torque waveform of both motors.

IV. CONCLUSION

As seen, most calculations are done offline in the inner and outer loop controllers based on MPC. Consequently, the control signals in each sampling interval are calculated in a very short time. Therefore, it is possible to use inexpensive microcontrollers. It also frees up microcontroller capacity to perform observer calculations in sensorless controls. The entire locus of the voltage space vector has been evaluated in the ICS-MPC method to prove the optimality of the used method. The results show that the proposed drive technique not only calculates the control signals in which ultimately leads to the realization of the comprehensive minimum cost function but also is independent of unwanted variations in motor parameters. Furthermore, the obtained control signals are independent of electric motor types. Indeed, the control signal of the outer loop can be applied in all of the electric motors with a smooth pole rotor. The inner loop control signal can also be applied to regulate the currents of any electric motor provided that the M matrix is reversible. It can be concluded that, in MIDP systems, the overall performance of the designed controllers has been far better than the conventional model-based control method.

APPENDIX:

The coefficients $\rho_1, \rho_2, \rho_3, \rho_4$ and M equations are as follows:

$$\rho_1 = [\rho_4 Q_f + Q\tau_p]; \quad \rho_2 = (I + A(X(t_i))\tau_p);$$
$$\rho_3 = BR^{-1}B^T\tau_p; \quad \rho_4 = (I + A^T(X(t_i))\tau_p);$$
$$M = I + \rho_3\rho_1; \quad A = \begin{bmatrix} \gamma_{11} & \gamma_{12} \\ \gamma_{21} & \gamma_{22} \end{bmatrix};$$
$$B = \frac{1}{L}\begin{bmatrix} 1 & 0 & 1 & 0 \\ 0 & 1 & 0 & 1 \end{bmatrix}^T;$$

In addition, the components of M matrix are as follows:

$$m_{11} = \left(\frac{\tau_p}{L}\right)^2 \left(\frac{Q_{11}}{R_{11}} + \frac{Q_{f11}}{R_{11}}\left(\frac{1}{\tau_p} - \frac{r_s}{L}\right)\right);$$

$$m_{12} = \left(\frac{\tau_p}{L}\right)^2 \frac{Q_{f22}}{R_{11}} \omega_{r1}(t_i);$$

$$m_{21} = -\left(\frac{\tau_p}{L}\right)^2 \frac{Q_{f11}}{R_{22}} \omega_{r1}(t_i);$$

$$m_{13} = \left(\frac{\tau_p}{L}\right)^2 \left(\frac{Q_{33}}{R_{11}} + \frac{Q_{f33}}{R_{11}}\left(\frac{1}{\tau_p} - \frac{r_s}{L}\right)\right);$$

$$m_{14} = \left(\frac{\tau_p}{L}\right)^2 \frac{Q_{f44}}{R_{11}} \omega_{r1}(t_i);$$

$$m_{23} = -\left(\frac{\tau_p}{L}\right)^2 \frac{Q_{f33}}{R_{22}} \omega_{r1}(t_i);$$

$$m_{22} = \left(\frac{\tau_p}{L}\right)^2 \left(\frac{Q_{22}}{R_{22}} + \frac{Q_{f22}}{R_{22}}\left(\frac{1}{\tau_p} - \frac{r_s}{L}\right)\right);$$

$$m_{24} = \left(\frac{\tau_p}{L}\right)^2 \left(\frac{Q_{44}}{R_{22}} + \frac{Q_{f44}}{R_{22}}\left(\frac{1}{\tau_p} - \frac{r_s}{L}\right)\right);$$

REFERENCES

[1] A. Plunkett and D. Plette, "Inverter-induction motor drive for transit cars," *IEEE Transactions on Industry Applications,* no. 1, pp. 26-37, 1977.

[2] J. M. Lazi, Z. Ibrahim, M. H. N. Talib, and R. Mustafa, "Dual motor drives for PMSM using average phase current technique," in *2010 IEEE International Conference on Power and Energy*, 2010: IEEE, pp. 786-790.

[3] A. A. A. Samat, D. Ishak, and S. Iqbal, "Voltage Space Vector Averaging Technique for Two PMSMs Connected in Parallel," *Int. J. Electr. Energy,* vol. 1, no. 4, pp. 234-238, 2013.

[4] Y. Matsumoto, S. Ozaki, and A. Kawamura, "A novel vector control of single-inverter multiple-induction-motors drives for Shinkansen traction system," in *APEC 2001. Sixteenth Annual IEEE Applied Power Electronics Conference and Exposition (Cat. No. 01CH37181)*, 2001, vol. 1: IEEE, pp. 608-614.

[5] J. M. Lazi, Z. Ibrahim, and M. Sulaiman, "Mean and diffrential torque control using hysteresis current controller for dual PMSM drives," in *Journal of Theoretical and Applied information Technology*, 2011: Citeseer.

[6] A. Del Pizzo, D. Iannuzzi, and I. Spina, "High performance control technique for unbalanced operations of single-vsi dual-PM brushles motor drives," in *2010 IEEE International Symposium on Industrial Electronics*, 2010: IEEE, pp. 1302-1307.

[7] G. Brando, L. Piegari, and I. Spina, "Simplified optimum control method for monoinverter dual parallel PMSM drive," *IEEE Transactions on Industrial Electronics,* vol. 65, no. 5, pp. 3763-3771, 2017.

[8] F. Xu, L. Shi, and Y. Li, "The weighted vector control of speed-irrelevant dual induction motors fed by the single inverter," *IEEE transactions on power electronics,* vol. 28, no. 12, pp. 5665-5672, 2013.

[9] D. Bidart, M. Pietrzak-David, P. Maussion, and M. Fadel, "Mono inverter dual parallel PMSM-structure and control strategy," in *2008 34th Annual Conference of IEEE Industrial Electronics*, 2008: IEEE, pp. 268-273.

[10] M. Ebadpour, M. B. B. Sharifian, and E. Babaei, "Modeling and control of dual parallel BLDC motor drive system with single inverter," in *2017 International Electrical Engineering Congress (iEECON)*, 2017: IEEE, pp. 1-4.

[11] Y. Lee and J.-I. Ha, "Control method for mono inverter dual parallel surface-mounted permanent-magnet synchronous machine drive system," *IEEE Transactions on Industrial Electronics,* vol. 62, no. 10, pp. 6096-6107, 2015.

[12] Y. Lee and J.-I. Ha, "Control method for mono inverter dual parallel interior permanent magnet synchronous machine drive system," in *2015 IEEE Energy Conversion Congress and Exposition (ECCE)*, 2015: IEEE, pp. 5256-5262.

[13] Y. Lee and J.-I. Ha, "Control method of monoinverter dual parallel drive system with interior permanent magnet synchronous machines," *IEEE*

Transactions on Power Electronics, vol. 31, no. 10, pp. 7077-7086, 2015.

[14] T. LIU and M. FADEL, "A Controller Proposed for Mono-Inverter Multiple-PMSM system," 2017.

[15] T. Liu, X. Ma, F. Zhu, and M. Fadel, "Reduced-Order Feedback Linearization for Independent Torque Control of a Dual Parallel-PMSM System," *IEEE Access,* vol. 9, pp. 27405-27415, 2021.

[16] K. Belda, "Study of predictive control for permanent magnet synchronous motor drives," in *2012 17th International Conference on Methods & Models in Automation & Robotics (MMAR)*, 2012: IEEE, pp. 522-527.

[17] P. ML, K. Eshwar, and V. K. Thippiripati, "A modified duty-modulated predictive current control for permanent magnet synchronous motor drive," *IET Electric Power Applications,* 2021.

[18] Y. Han, C. Gong, L. Yan, H. Wen, Y. Wang, and K. Shen, "Multiobjective finite control set model predictive control using novel delay compensation technique for PMSM," *IEEE Transactions on Power Electronics,* vol. 35, no. 10, pp. 11193-11204, 2020.

[19] E. S. De Santana, E. Bim, and W. C. do Amaral, "A predictive algorithm for controlling speed and rotor flux of induction motor," *IEEE Transactions on Industrial Electronics,* vol. 55, no. 12, pp. 4398-4407, 2008.

[20] Y. Zhang, X. Wang, H. Yang, B. Zhang, and J. Rodriguez, "Robust predictive current control of induction motors based on linear extended state observer," *Chinese Journal of Electrical Engineering,* vol. 7, no. 1, pp. 94-105, 2021.

[21] J. Kim, Y. Bak, and K.-B. Lee, "Control strategy of the mono converter dual parallel surface-mounted permanent magnet synchronous generator in wind power generation system," in *2016 IEEE International Conference on Power and Energy (PECon)*, 2016: IEEE, pp. 461-466.

[22] M. Jafari, K. Abbaszadeh, and M. MOHAMADIAN, "A novel DTC-SVM approach for two parallel-connected induction motors fed by matrix converter," *Turkish Journal of Electrical Engineering & Computer Sciences,* vol. 26, no. 3, pp. 1599-1611, 2018.

[23] N. L. Nguyen, M. Fadel, and A. Llor, "Predictive Torque Control-A solution for mono inverter-dual parallel PMSM system," in *2011 IEEE International Symposium on Industrial Electronics*, 2011: IEEE, pp. 697-702.

[24] T. Liu and M. Fadel, "An efficiency-optimal control method for mono-inverter dual-PMSM systems," *IEEE Transactions on Industry Applications,* vol. 54, no. 2, pp. 1737-1745, 2017.

[25] Š. Janouš, J. Talla, Z. Peroutka, and V. Šmídl, "Predictive Control of Parallel Induction Motors Fed by Single Inverter with Common Current Sensors," in *IECON 2018-44th Annual Conference of the IEEE Industrial Electronics Society*, 2018: IEEE, pp. 5843-5848.

[26] M. A. Abbasi and A. R. B. HUSAIN, "Model predictive control of a dual induction motor drive fed by a single voltage source inverter," *Turkish Journal of*

Electrical Engineering & Computer Sciences, vol. 26, no. 3, pp. 1623-1637, 2018.

[27] N. L. Nguyen, M. Fadel, and A. Llor, "A new approach to predictive torque control with dual parallel PMSM system," in *2013 IEEE International Conference on Industrial Technology (ICIT)*, 2013: IEEE, pp. 1806-1811.

[28] G. Cimini, D. Bernardini, A. Bemporad, and S. Levijoki, "Online model predictive torque control for permanent magnet synchronous motors," in *2015 IEEE International Conference on Industrial Technology (ICIT)*, 2015: IEEE, pp. 2308-2313.

[29] A. BOUARFA and M. FADEL, "Optimal predictive torque control of two PMSM supplied in parallel on a single inverter," *IFAC-PapersOnLine,* vol. 48, no. 30, pp. 84-89, 2015.

[30] T. Liu and M. Fadel, "Performance comparison of control strategies for mono-inverter dual-PMSM system," in *2016 IEEE International Power Electronics and Motion Control Conference (PEMC)*, 2016: IEEE, pp. 637-642.

[31] A. Cervone, L. Di Noia, R. Rizzo, I. Spina, and R. Miceli, "A Constrained Optimal Model Predictive Control for Mono Inverter Dual Parallel PMSM Drives," in *2018 7th International Conference on Renewable Energy Research and Applications (ICRERA)*, 2018: IEEE, pp. 1501-1507.

[32] W. Cai, X. Wu, M. Zhou, Y. Liang, and Y. Wang, "Review and Development of Electric Motor Systems and Electric Powertrains for New Energy Vehicles," *Automotive Innovation,* vol. 4, no. 1, pp. 3-22, 2021.

[33] K. Koiwa, T. Kuribayashi, T. Zanma, K.-Z. Liu, and M. Wakaiki, "Optimal current control for PMSM considering inverter output voltage limit: model predictive control and pulse-width modulation," *IET Electric Power Applications,* vol. 13, no. 12, pp. 2044-2051, 2019.

[34] H. Wan, Y. Pan, and J. Huang, "Comparative Study of VC and DTC for Single-Inverter Dual-Motor System," *International Journal of Digital Content Technology and its Applications,* vol. 6, no. 18, p. 587, 2012.

[35] N. Tauchnitz, "The Pontryagin maximum principle for nonlinear optimal control problems with infinite horizon," *Journal of Optimization Theory and Applications,* vol. 167, no. 1, pp. 27-48, 2015.